J. Mod. Opt. **47**, 1713-28 (2000), (C) 2000 Taylor & Francis Ltd.

Observation of Sub-kilohertz Resonance in Rf-Optical Double Resonance Experiment in Rare Earth Ions in Solids

M.K. Kim [a], B.S. Ham [b], P.R. Hemmer [c], and M.S. Shahriar [b]

[a] *Dept. of Physics, University of South Florida, Tampa, FL 33620*

[b] *Research Laboratory of Electronics, Massachusetts Institute of Technology, Cambridge, MA 02139, USA*

[c] *Rome Laboratory, Hanscom Air Force Base, MA 01731, USA*

Abstract

We have observed kHz and sub-kHz resonance structures in rf-optical double resonance experiments of rare-earth-doped solids, when the frequency of the rf field is scanned across the hyperfine transitions while monitoring the resonant optical absorption of a cw laser. The effect is observed only when the laser spectral width is broad compared to the hyperfine structure. The observed line widths are apparently free of the inhomogeneous widths of hyperfine levels and the line shape has peculiar double peak structure. The effect is modeled with a resonance involving three atomic levels interacting with three electromagnetic fields, two optical and one rf, in a triangular or 'delta' configuration. While the ordinary optical-rf two-field resonance is limited by spin inhomogeneous width, the simultaneous excitation of three coupled transitions lead to narrow and highly nonlinear resonance structures that does not get averaged by the inhomogeneous distribution of hyperfine transition.

J. Mod. Opt. **47**, 1713-28 (2000), (C) 2000 Taylor & Francis Ltd.

Observation of Sub-kilohertz Resonance in Rf-Optical Double Resonance Experiment in Rare Earth Ions in Solids

1. INTRODUCTION

We have observed a peculiarly narrow resonance structure in the course of optical-rf double resonance experiment of rare earth ions in solids. The resonance is characterized by a sharp double peak structure in the absorption spectrum as the rf frequency is scanned across the hyperfine transition, with the few kHz width of the transparency hole at least an order of magnitude narrower than the spin inhomogeneous width. The effect is evident only when the laser bandwidth is larger than the hyperfine level splittings. A theoretical model is presented based on the assumption that the optical fields of a noisy laser simultaneously couples an optically excited state with two hyperfine levels of the ground state, which in turn are acted on by the rf field. A quantum interference effect among the three coupled transitions creates sharp fringes in the frequency domain that does not get averaged out by ensemble average over the inhomogeneous broadening of the optical or spin transitions. The model is found to be consistent with the main features of the experimental observations.

Various quantum interference effects in atomic transitions have recently been the research topic of great interest, because of the rich and often counter-intuitive physics and their potential applications in nonlinear optical devices and spectroscopy. For example, in electromagnetically induced transparency (EIT) [1, 2], multiple paths of transitions created by the ac Stark effect of a strong coupling field can cause destructive interference and result in a transparency hole in the absorption spectrum. The effect is applied in the enhanced harmonic generation [3, 4], wave mixing[5, 6], and amplification and laser action without population

inversion [7, 8, 9]. Similar processes occur in coherent population trapping [10, 11, 12, 13] of resonant Raman interaction [14, 15], where the spin coherence created by Raman optical fields gives rise to quantum interference and transparency hole in the absorption spectrum. The spin coherence can be created by directly applying an rf field on the spin transition, and this also results in transparency [16]. In most of these systems, the basic process is an interaction of a three level system with two electromagnetic fields, where the two transitions or some linear combinations interfere against each other to create a characteristic transparency hole in the absorption spectrum. A general requirement for the observation of the transparency hole is that the coupling field be strong enough to overcome the inhomogeneous broadening. For example, in resonant Raman interference, the optical Raman Rabi frequency needs to be large compared to the hyperfine inhomogeneous width [15] in order for the coherent population trapping to produce observable hole in the absorption spectrum. A few authors have investigated interaction of closed loop of transitions including a triangular resonance [17, 18], but it appears these studies have been restricted to the cases of time-dependence and phase-dependence of the system response at exact resonance only.

There are a number of spectral line-narrowing processes that have made great contributions in the various areas of laser spectroscopy. Examples are laser induced fluorescence [19], spectral hole burning [20], Doppler-free spectroscopy by multiphoton processes [21], Ramsey resonance by separated fields [22], and various double resonance methods [23, 24]. Most often the strategy is to reduce or eliminate the effect of inhomogeneous broadening of the spectral lines, in order to reveal the natural or homogeneous line widths. The experiments described here started out as an optical-rf double resonance experiment, where the spectral line width is expected to be limited by the spin inhomogeneous width. The observed

narrow resonance structure and the proposed theoretical model of three-level three-field interaction allows spectral resolution even below the spin inhomogeneous line width.

2. EXPERIMENT

The experiments are performed using an apparatus shown in Fig. 1, with a ring dye laser that provides about 500 mW of output. An acoustooptic modulator is used to turn the laser pulses on and off. The laser light then enters the sample crystal in a liquid helium cryostat. A 15-turn rf coil is wound around the crystal and the transmitted light through the crystal is detected by a photodiode. The rf field, up to 30 MHz, for the coil is generated using a synthesized function generator, which is switched and amplified up to 2 W power. A digital delay generator provides the timing signals. The detected signal is fed into a lock-in amplifier or to a digital oscilloscope, and a desktop computer running LabView controls all the digital instruments, and collects and processes the data. Data presented below utilize three different detection methods. One is lock-in amplifier output of transmitted optical signal with pulsed optical field and cw rf field ('optical lock-in signal'); another is lock-in amplifier output with cw optical field and pulsed rf field ('rf lock-in signal'); and the third is the output of digital oscilloscope showing averaged time signal of photodiode ('time signal').

Fig. 2a) shows an example of the observed resonance structure when the transmitted light is lock-in detected while the rf frequency is scanned near the 7 MHz hyperfine transition of the $^3H_4$ ground state. The sample is 0.1 at. % Pr^{3+}:$YAlO_3$ of 17 mm length at temperature of 4.2 K. (See Refs. [23, 25, 26, 27, 28] for spectroscopic details of Pr^{3+}:$YAlO_3$.) The optical field is tuned to 610.53 nm $^3H_4$ — $^1D_2$ transition, where the optical density of the crystal is ~0.4, or 30% absorption. For most of the measurements the optical field is chopped by the AOM at 1 kHz

with 50 % duty cycle, while the rf field is cw. Note the very narrow 2.1 kHz transparency hole centered at 7.1162 MHz. The vertical scale is proportional to the transmitted light and the figure indicates close to 70% maximum absorption, relative to off-resonance background, on either side of the central hole, but almost complete transmission at the center of the hole. This was consistent with naked eye observation of the laser beam transmitted through the crystal. The structure disappears, however, when the laser frequency is stabilized to less than a few MHz, as shown in Fig. 2b), where the overall transmittance is higher compared to Fig. 2a) because of spectral hole burning. (Even when the laser frequency is slowly scanned to reduce the spectral hole burning effect, the above resonance structure is not observed.) The ground state hyperfine transitions are previously known to have center frequencies 7.057, 14.13, and 21.19 MHz with inhomogeneous widths of ~ 50 kHz. For comparison, Fig. 2c) shows the hyperfine inhomogeneous line at 7.06 MHz transition as detected by photon echo nuclear double resonance (PENDOR). We have also found similar structures near the others of these frequencies: 14.233 MHz and 21.349 MHz, with the respective gap widths of 3.0 and 3.5 kHz. Furthermore, we have observed 0.65 kHz gap structure at 10.433 MHz, Fig. 2d), and 1.0 kHz gap structure at 17.390 MHz in Pr^{3+}:Y_2SiO_5, where the corresponding known hyperfine frequencies are 10.19 and 17.30 MHz with inhomogeneous width of ~ 40 kHz [29, 30]. As indicated above, a very important observational peculiarity is that these narrow transparency hole structures appear only when the laser is known to have large bandwidth compared to the hyperfine transition frequencies. When the laser stabilization circuit is locked to reduce the bandwidth to a few MHz or less, the kHz hole structures disappear. The laser frequency structure is monitored with a Fabry-Perot interferometer to have about 40 MHz bandwidth when the stabilization was inactive, with additional fluctuation over ~100 MHz range. When the stabilization is locked the laser

bandwidth is measured to be at most 3~4 MHz, and had occasional mode-hops. The laser cavity mode spacing is 240 MHz.

We have experimentally studied the behavior of the resonance structure with respect to a number of experimental parameters. For example, Fig. 3 shows that the increasing rf field strength broadens the width of the side wings proportionately, but the width of the gap remains constant. The rf circuit is not resonant or matched but if we assume a few gauss of rf magnetic field strength and 2.4 kHz/G gyromagnetic ratio of the $^3H_4$ hyperfine levels, the spin Rabi frequency is expected to be a few kHz. Figure 4 shows the behavior when the optical field strength is varied using neutral density filters. There is a moderate but clear increase of the gap width as the optical power increases. The optical power that enters the sample is about 10 mW and the 2-mm diameter beam is focussed by a 30 cm lens. If we assume a ratio (atomic homogeneous width)/(laser spectral width) = 10^{-4} and oscillator strength of 3 x 10^{-7}, the optical Rabi frequency is ~3 kHz. Fig. 5 shows the evolution of resonance lineshape as the pulse length is increased. The rf lock-in signal has zero background and the resonance curve displays distinct and reproducible structures. The rf pulse length is varied from 100 μs to 800 μs while the repetition rate is kept at 1 kHz. One can see the establishment of the resonance structure in a few hundred μs. Notice also the high degree of symmetry of the detailed lineshape with respect to the center of the resonance. The high 'frequency' wiggle is due to the 1 kHz lock-in cycle. In order to ascertain that the main features of these observations are not artifacts of lock-in detection, we have acquired 2.0 ms long time signal, averaged 300 shots at 100 Hz repetition rate, of the transmitted light using a digital oscilloscope, then scanned the rf frequency from 7.11 to 7.13 MHz in 0.5 kHz steps, to compose a time-frequency profile of the resonance structure. A result is shown in Fig. 6a), where basically all the features of the frequency-domain data are

reproduced, including the gradual sharpening of the double peak structure as a function of time. Figure 7 shows a few of individual time signal traces for various rf frequencies. Further observational notes are that the observed resonance structure disappears quite abruptly when the temperature rises beyond 10 K, and that we have looked for similar effects in Pr^{3+}:LaF_3 but found none. We have also measured the resonance structure vs. rf frequency at various optical detuning, and only observed variations in overall signal size and some detailed shapes of the central peaks.

3. THEORY

We propose to model the observed resonance effect as a three-level atomic system interacting with three electromagnetic fields (3L3F) in a delta-shape configuration, as shown in Fig. 8. The system consists of two hyperfine levels |1> and |2> of the ground state, with eigen energies ε_i (i = 1, 2), and an optically excited level |3>, with $\varepsilon_3 = 0$. The optical field is $E = \frac{1}{2}\left\{E_1 e^{-i\omega_1 t} + E_2 e^{-i\omega_2 t}\right\} + \text{c.c.}$ and we assume that E_i's couple the |i>–|3> transitions independently, with Rabi frequencies $\Omega_i = \frac{p_i E_i}{2\hbar}$ (p_i: |i>–|3> transition electric dipole moments) and detuning parameters $\Delta_i = (\varepsilon_3 - \varepsilon_i)/\hbar - \omega_i$. (Note that the definition of Rabi frequency here is one half of more conventional definition.) These transitions have population relaxation rates Γ_i, and phase relaxation rates γ_i. The two ground states |1>–|2> are coupled by the rf magnetic field, with similarly defined parameters: field frequency, ω'; Rabi frequency of magnetic dipole transition, Ω'; detuning, $\Delta' = (\varepsilon_2 - \varepsilon_1)/\hbar - \omega'$; population relaxation rate, Γ'; and phase relaxation rate γ'.

The density matrix equation of motion [31, 32]

$$\frac{d}{dt}\rho_\omega = -\frac{i}{\hbar}\left[\mathrm{H}_\omega, \rho_\omega\right] + (\textit{relaxation terms}) \tag{1}$$

is written in a rotating reference frame defined with

$$U_\omega = \begin{bmatrix} \mathrm{e}^{-i\omega_1 t} & 0 & 0 \\ 0 & \mathrm{e}^{-i\omega_2 t} & 0 \\ 0 & 0 & 1 \end{bmatrix} \tag{2}$$

so that

$$\rho_\omega = U_\omega \rho U_\omega^{-1} \equiv \begin{bmatrix} \rho_1 & \sigma' & \sigma_1 \\ \sigma'^{*} & \rho_2 & \sigma_2 \\ \sigma_1^{*} & \sigma_2^{*} & \rho_3 \end{bmatrix}, \tag{3}$$

where $\rho = |\Psi\rangle\langle\Psi|$ is the density matrix in the lab frame. The Hamiltonian in this rotating frame is, with the three-photon resonance detuning $\delta = \Delta' - (\Delta_1 - \Delta_2)$,

$$\begin{aligned} \mathrm{H}_\omega &= U_\omega \mathrm{H} U_\omega^{-1} + i\hbar\left(\frac{d}{dt}U_\omega\right)U_\omega^{-1} \\ &= \begin{bmatrix} -\hbar\Delta_1 & -\hbar\Omega' \mathrm{e}^{-i\delta t} & -\hbar\Omega_1 \\ -\hbar\Omega' \mathrm{e}^{i\delta t} & -\hbar\Delta_2 & -\hbar\Omega_2 \\ -\hbar\Omega_1 & -\hbar\Omega_2 & 0 \end{bmatrix}. \end{aligned} \tag{4}$$

The rotating wave approximation is used where we neglect the terms of frequencies $2\omega_1$ and $2\omega_2$ compared to dc terms, as well as the terms of frequency $(\omega_1 - \omega_2 + \omega')$ compared to $\delta = (\omega_1 - \omega_2$

– ω'). Notice that this Hamiltonian is time-dependent. For a three-level three-field system, it is in general not possible to find a rotating frame that completely removes the time-dependence of the Hamiltonian. The explicit form of the equations of motion (1) is written out as:

$$\begin{cases} \dot{\rho}_1 = -i\Omega_1\left(\sigma_1 - \sigma_1^*\right) - i\Omega'\left(\mathrm{e}^{+i\delta t}\sigma' - \mathrm{e}^{-i\delta t}\sigma'^*\right) + \Gamma_1\rho_3 - \tfrac{1}{2}\Gamma'\left(\rho_1 - \rho_2\right) \\ \dot{\rho}_2 = -i\Omega_2\left(\sigma_2 - \sigma_2^*\right) + i\Omega'\left(\mathrm{e}^{+i\delta t}\sigma' - \mathrm{e}^{-i\delta t}\sigma'^*\right) + \Gamma_2\rho_3 + \tfrac{1}{2}\Gamma'\left(\rho_1 - \rho_2\right) \\ \dot{\rho}_3 = +i\Omega_1\left(\sigma_1 - \sigma_1^*\right) + i\Omega_2\left(\sigma_2 - \sigma_2^*\right) - \left(\Gamma_1 + \Gamma_2\right)\rho_3 \\ \dot{\sigma}_1 = -i\Omega_1\left(\rho_1 - \rho_3\right) + i\Omega'\mathrm{e}^{-i\delta t}\sigma_2 - i\Omega_2\sigma' - \left(\gamma_1 - i\Delta_1\right)\sigma_1 \\ \dot{\sigma}_2 = -i\Omega_2\left(\rho_2 - \rho_3\right) + i\Omega'\mathrm{e}^{+i\delta t}\sigma_1 - i\Omega_1\sigma'^* - \left(\gamma_2 - i\Delta_2\right)\sigma_2 \\ \dot{\sigma}' = -i\Omega'\mathrm{e}^{-i\delta t}\left(\rho_1 - \rho_2\right) - i\Omega_2\sigma_1 + i\Omega_1\sigma_2^* - \left(\gamma' - i\left(\Delta_1 - \Delta_2\right)\right)\sigma' \end{cases} \tag{5}$$

Because of the time-dependence, it is not possible to write a formal solution to the density matrix equation using matrix exponential, and it appears rather difficult to discern the general behavior of the solution. However, an analogy with a single-function equation of motion, in the form $\frac{dz}{dt} = \left[-\gamma + i\Omega + i\Omega' e^{i\delta t}\right] z(t)$ may be made whose solution contains a factor for example $z \sim \cos\left[\frac{\sin\delta t}{\delta/\Omega'}\right]$. Because of the sinc function argument in the cosine, there are rapid oscillations as δ approaches zero. Numerical calculation of the three-level system displays analogous behavior, as will be seen below. This rapid oscillation washes out any inhomogeneous distribution of the detuning parameter δ, except at the exact center of the distribution.

The equation of motion (Eq. 5) is solved numerically using Runge-Kutta method on MatLab. A single-atom solutions are then accumulated over the inhomogeneous distribution of the spin and optical transitions. The level |3> population ρ_3 is plotted as a measure of optical

absorption, as a function of rf detuning Δ'. The top trace of Fig. 9a) shows a result of such calculation. The separation of the double peak is the Raman Rabi frequency $2\Omega = 2\sqrt{\Omega_1^2 + \Omega_2^2}$. On top of the double peak structure, there is a rapid oscillation in frequency domain with period of 1/2t. The width of each of the double peaks is proportional to the spin Rabi frequency, but the optical dephasing γ also broadens it. Also note that the center of the resonance is exactly zero with respect to the off-resonance background. (For the top trace of Fig. 9a) the off-resonance background level is ρ_3 = 0.217 and the peak level is 0.226, so that the peak represents < 5% change in calculated ρ_3.) This 3L3F solution is contrasted with a three-level two-field (3L2F) solution in Fig. 9b), where there are one optical and one rf fields, corresponding to a normal optical-rf double resonance experiment. Again the double peak separation corresponds to optical Rabi frequency for ac Stark effect. Note that there is no rapid oscillation structure, and that the resonance center is above zero with respect to the off-resonance background. There appear marked differences between the two-field and three-field solutions when they are integrated over the inhomogeneous broadening of atoms. For the 3L2F case, the double peak structure is smeared out immediately when it is integrated over the spin inhomogeneous width and the integrated resonance curve has the spin inhomogeneous width. On the other hand, there is no qualitative change in the resonance shape of 3L3F solution when it is integrated over the spin inhomogeneous width. When integrated over the optical broadening, the gap between the double peak narrows but remains non-zero. One also notices that there is a qualitative change in the resonance line shape and that the center of resonance is still zero with respect to the off-resonance background.

Next let us examine the behavior of the 3L3F solution, integrated over optical inhomogeneous width, with respect to various parameters. Fig. 10 shows its dependence on the

spin Rabi frequencies. As the spin Rabi frequency increases, the width of the wings increase proportionately and the amplitude of the signal increases as the square of the Rabi frequency, but the width of the gap does not change. The increase of optical Rabi frequency results, Fig. 11, in the proportionate increase of the gap width. On the other hand, the numerical experiments show that the gap width and structure are also dependent on the phase relaxation rates of the spin and optical transitions. In Fig. 12, the increase in spin phase relaxation rate γ' results in reduction of overall resonance structure but the resonance widths remain the same. Quite unexpectedly however, when the optical phase relaxation rate γ is increased in Fig. 13, the resonance structure becomes narrower and sharper. The population relaxation rates Γ's do not affect the resonance shape appreciably. Figure 6b) shows the time-frequency plot of the resonance for a particular set of parameters indicated in the caption.

4. DISCUSSION

The numerical analysis based on the model of three-level atoms interacting with three electromagnetic fields has several important features that are consistent with the experimental observations. First, the resonance lineshape has the distinct double-peak structure. The width of the gap is very small compared to the inhomogeneous width of the spin transition. This double peak structure is averaged out and absent in the case of two-field rf-optical double resonance. Also notice that the shape of the calculated resonance structure, integrated over optical linewidth, has the distinct shape observed experimentally. Second, there is the fringe pattern in the frequency domain with "period" equal to the inverse of the pulse length. Third, the increase of the width of the wings with respect to the rf field strength is well verified by the experiment. With an estimated few gauss of rf magnetic field strength and 2.4 kHz/G gyromagnetic ratio of

the $^3H_4$ hyperfine levels, the spin Rabi frequency is expected to be a few kHz. Although the magnetic field is not calibrated, at least the order of magnitude appears reasonable. But more importantly, the wing width does increase in proportion with the field strength. As for the dependence of the gap width on the optical Rabi frequency, the experimental data shows much slower than linear dependence seen in the theory. One may attribute this tentatively to the effect of the optical phase relaxation. The gap width calculated according to the theoretical model appears to be determined by the optical Rabi frequency, but the optical phase relaxation also narrows the gap width. This behavior is very nonlinear and it is difficult to predict the gap width in terms of experimental parameters, except to say that the maximum gap width is proportional to the optical Rabi frequency. Some of the numerical results suggest that the optical phase relaxation attenuates the rapid oscillation in the vicinity of the resonance and thereby reduces the range of frequency where the singular oscillation due to three-photon resonance is effective, and results in the narrowing of the resonance structure. Another point of difficulty is that the observed center frequency of resonance is some tens of kHz away from the previously known hyperfine frequencies, and it also varies by a few kHz between different experimental runs.

The three-level three-field model seems to offer at least partial explanations for the observed peculiar resonance structure. The model also seems intuitively reasonable in that there is a singularity of some sort when three transitions form a closed loop resonance. As with a set of three coupled mechanical oscillators, the three driving fields need to have exact frequency and phase match in order to sustain the oscillation. On the other hand, the model assumes two simultaneous cw monochromatic fields, whereas in a real dye laser the instantaneous spectrum of the laser may be more likely single mode with occasional mode hop. Therefore, we may modify the model by allowing only a single optical field with fluctuating frequency. But if the

fluctuation is faster than the optical phase relaxation time, then an optical transition will retain the laser phase memory while the laser jumps back and forth between different frequencies. A simple numerical calculation with two non-overlapping laser pulses each resonant with one of the two optical transitions shows that the singular oscillatory behavior persists as far as the delay between the two pulses is not longer than the optical phase relaxation time. In this regard, one may note that among the three samples that we have studied, Pr^{3+} in $YAlO_3$ (T_2 = 35 μs), YSO (110 μs), and LaF_3 (6 μs), we have not observed the resonance structure in LaF_3. Also note that quite often the laser fluctuation can be approximated as a contribution to the optical phase relaxation. A systematic development of the revised model with fluctuating field needs to be carried out.

In summary, we have observed a peculiar resonance structure in a rf-optical double resonance experiment of rare earth-doped crystals, characterized by a double peak structure of only a few kHz width. A numerical study based on a model consisting of three-level atoms interacting with three simultaneous electromagnetic fields shows some of the main features consistent with the experimental data, such as the peculiar resonance lineshape and its dependence on the rf and optical Rabi frequencies.

ACKNOWLEDGEMENT

This work is supported by the National Science Foundation (grant ECS 9421304) and the U.S. Air Force Office of Scientific Research (grant F49620-96-1-0395).

REFERENCES

[1] S.E. Harris, G.Y. Yin, A. Kasapi, M. Jain, and Z.F. Luo, "Electromagnetically induced transparency", in *Coherence and Quantum Optics VII*, J.H. Eberly, L. Mandel, and E. Wold, eds. (Plenum, 1996), pp.295-304.

[2] K. J. Boller, A. Imamoglu, and S. E. Harris, "Observation of electromagnetically induced transparency", Phys. Rev. Lett. **66**, 2593-6 (1991).

[3] S. E. Harris, J. E. Field, and A. Imamoglu, "Nonlinear optical processes using electromagnetically induced transparency", Phys. Rev. Lett. **64**, 1107-10 (1990).

[4] G. Z. Zhang, K. Hakuta, and B.P. Stoicheff, "Nonlinear optical generation using electromagnetically induced transparency in atomic hydrogen", Phys. Rev. Lett. **71**, 3099-102 (1993).

[5] Y. Li and M. Xiao, "Enhancement of nondegenerate four-wave mixing based on electromagnetically induced transparency in rubidium atoms", Opt. Lett. **21**, 1064-6 (1996).

[6] B.S. Ham, M.S. Shahriar, and P.R. Hemmer, "Enhanced nondegenerate four-wave mixing owing to electromagnetically induced transparency in a spectral hole-burning crystal", Opt. Lett. **22**, 1138-40 (1997).

[7] B.S. Ham, M.S. Shahriar, and P.R. Hemmer, "Radio-frequency-induced optical gain in Pr^{3+}:Y_2SiO_5", J. Opt. Soc. Am. B **15**, 1541-44, (1998).

[8] M.O. Scully, S. Y. Zhu, and A. Gavrielides, "Degenerate quantum-beat laser: Lasing without inversion and inversion without lasing", Phys. Rev. Lett. **62**, 2813-6 (1989).

[9] S. E. Harris, "Lasers without inversion: Interference of lifetime-broadened resonances", Phys. Rev. Lett. **62**, 1033-6 (1989).

[10] G. Alzetta, A. Gozzini, L. Moi, and G. Orriols, "An experimental method for the observation of rf transitions and laser beat resonances in oriented Na vapour", Nuovo Cimento **36**, 5-20 (1976).

[11] H. R. Gray, R. M. Whitley, and C. R. Stroud Jr., "Coherent trapping of atomic population", Opt. Lett. **3**, 218-20 (1978).

[12] P.R. Hemmer, K.Z. Cheng, J. Kierstead, M.S. Shahriar, and M.K. Kim, "Time-domain optical data storage by use of Raman coherent population trapping", Opt. Lett. **19**, 296-8 (1994).

[13] B.S. Ham, P.R. Hemmer, and M.S. Shahriar, "Efficient electromagnetically induced transparency in a rare-earth doped crystal", Opt. Comm. **144**, 227-30 (1997).

[14] R. G. Brewer and E. L. Hahn, "Coherent Two-Photon Processes: Transient and Steady-State Cases", Phys. Rev. A **11**, 1641-9 (1975).

[15] M. S. Shahriar and P. R. Hemmer, "Direct excitation of microwave-spin dressed states using a laser-excited resonance Raman interaction", Phys. Rev. Lett. **65**, 1865-8 (1990).

[16] Y. Zhao, C. Wu, B.-S. Ham, M. K. Kim, and E. Awad, "Microwave induced transparency in ruby", Phys. Rev. Lett. **79**, 641-4 (1997).

[17] S.J. Buckle, S.M. Barnett, P.L. Knight, M.A. Lauder, and D.T. Pegg, "Atomic interferometers: Phase-dependence in multilevel atomic transitions", Optica Acta **33**, 1129-40 (1986).

[18] M.J. Lim, T.H. Stievater, P.H. Bucksbausm, and R.S. Conti, "Population dynamics of a triply driven, three-level atomic system", Bull. Am. Phys. Soc. **44**, 584 (APS Centennial Meeting, Atlanta, GA, Mar. 1999).

[19] M.S. Feld and A. Javan, "Laser-induced line-narrowing effects in coupled Doppler-broadened transitions", Phys. Rev. **177**, 540-62 (1969).

[20] R. M. Macfarlane and R. M. Shelby, "Measurement of Nuclear and Electronic Zeeman Effects Using Optical Hole-Burning Spectroscopy", Opt. Lett. **6**, 96-8 (1981).

[21] M.M. Salour and C. Cohen-Tannoudji, "Observation of Ramsey's interference fringes in the profile of Doppler-free two-photon resonances", Phys. Rev. Lett. **38**, 757-60 (1977).

[22] J. E. Thomas, P. R. Hemmer, S. Ezekiel, C. C. Leiby, R. H. Picard, and C. R. Willis, "Observation of Ramsey fringes using a stimulated, resonance Raman transition in a sodium atomic beam", Phys. Rev. Lett. **48**, 867-70 (1982).

[23] R. M. Shelby, R. M. Macfarlane, and R. L. Shoemaker, "Two-Pulse Photon Echo Electron-Nuclear Double Resonance of $YAlO_3$:Pr^{3+}", Phys. Rev. B **25**, 6578-83 (1982).

[24] R. M. Shelby, C. S. Yannoni, and R. M. Macfarlane, "Optically Detected Coherent Transients in Nuclear Hyperfine Levels", Phys. Rev. Lett. **41**, 1739-42 (1978).

[25] L. E. Erickson, "Hyperfine Interaction in the Lowest Levels of the $^3H_4$ and $^1D_2$ States of Trivalent Praseodymium in Yttrium Aluminum Perovskite ($YAlO_3$)", Phys. Rev. B **19**, 4412-20 (1979).

[26] R. M. Macfarlane, R. M. Shelby, and R. L. Shoemaker, "Ultrahigh-Resolution Spectroscopy: Photon Echoes in $YAlO_3:Pr^{3+}$ and $LaF_3:Pr^{3+}$", Phys. Rev. Lett. **43**, 1726-9 (1979).

[27] M. Mitsunaga, R. Yano, and N. Uesugi, "Stimulated-photon-echo spectroscopy. II. Echo modulation in $Pr^{3+}:YAlO_3$", Phys. Rev. B **45**, 12760-8 (1992).

[28] M. Mitsunaga, "Kilohertz-resolution pump-probe spectroscopy in $Pr^{3+}:YAlO_3$", Opt. Lett. **18**, 1256-8 (1993).

[29] K. Holliday, M. Croci, E. Vauthey, and U.P. Wild, "Spectral hole burning and holography in an $Y_2SiO_5:Pr^{3+}$ crystal", Phys. Rev. B **47**, 14741-52 (1993).

[30] R.W. Equall, R.L. Cone, and R.M. Macfarlane, "Homogeneous broadening and hyperfine structure of optical transitions in $Pr^{3+}:Y_2SiO_5$", Phys. Rev. B **52**, 3963-9 (1995).

[31] P.R. Hemmer, M.S. Shahriar, V.D. Natoli, and S Ezekiel, "Ac-Stark shifts in a two-zone Raman interaction", J. Opt. Soc. Am. B **6**, 1519-28 (1989).

[32] H. Sonajalg and M.K. Kim, "Perturbation analysis of Raman echo", J. Opt. Soc. Am. B **15**, 1780-91 (1998).

FIGURES

Fig. 1: Schematic of apparatus. RDL: ring dye laser; AOM: acoustooptic modulator; S: sample crystal with rf coil inside a liquid helium cryostat; D: photodiode; DDG: digital delay generator; SFG: synthesized function generator; VCO: voltage controlled oscillator; SW: rf switch; AMP: 2W rf amplifier; DSO: digital oscilloscope; LIA: lock in amplifier; PC: desktop computer controlling digital devices (*).

Fig. 2: a) Optical lock-in signal, in arbitrary units, vs. rf frequency for $^3H_4$ to $^1D_2$ transition in Pr^{3+}:$YAlO_3$ near 7 MHz when the laser is not stabilized, and b) when the laser is stabilized. For optical lock-in signal the optical field is pulsed at 1 kHz rate with 50% duty cycle while the rf field is cw. c) The stimulated photon echo signal vs. frequency of rf pulse applied during the 100 μs period between the second and third pulses of stimulated photon echo experiment. d) Optical lock-in signal vs. rf frequency for $^3H_4$ to $^1D_2$ transition in Pr^{3+}:Y_2SiO_5 near 10 MHz.

Fig. 3: Optical lock-in signal vs. rf frequency for varying rf field strengths. Relative rf field amplitudes, from top to bottom, is nominally 1:2:4:8:16. (Different lock-in amplifier gains have been used between different traces, so that the relative vertical scales should not be compared between them. The glitch on the right end of top trace is an experimental artifact.)

Fig. 4: Optical lock-in signal vs. rf frequency for varying optical field strengths. Neutral density filters of optical density, from top to bottom, 0.04, 0.5, 1.0, 1.5, and 2.0 are inserted before the sample. Another set of neutral density filters are used in front of the detector to adjust detectable signal levels.

Fig. 5: Rf lock-in signal vs. rf frequency for varying rf pulse length. For rf lock-in signal the optical field is cw while rf field is pulsed at 1 kHz. The rf pulse lengths are, from top to bottom, 100, 200, 300, 400, 500, 600, 700, and 800 μs.

Fig. 6: Oscilloscope time signal of transmitted light when 5 ms long rf pulse is applied. The rf frequencies are, from top to bottom, 7110, 7111, 7112, 7113, 7114, and 7115 kHz. The horizontal scale is 1 ms/div and the signals are averaged for 1000 sweeps.

Fig. 7: a) Experimental and b) calculated profiles of optical signals vs. time and rf frequency. The vertical scale in a) is the photodiode voltage measured on the oscilloscope, and in b) it is the population of level |3>, which is inverted in order to represent higher absorption with larger |3> state population. The parameters used in b) are: $\Gamma_1 = \Gamma_2 = 1$, $\Gamma' = 0$; $\gamma_1 = \gamma_2 = 2\pi$; $\gamma' = 0.4\pi$; $\Omega_1 = \Omega_2 = 4\pi$; $\Omega' = 0.2\pi$; integrated over optical inhomogeneous width of 20, in steps of 0.5 and spin inhomogeneous width of 10, in steps of 0.5. The FREQ axis is $\Delta'/2\pi$.

Fig. 8: A three-level three-field (3L3F) system.

Fig. 9: a) Calculated profile of 3L3F resonance, ρ_3 vs. $\Delta'/2\pi$. Top: Single atom calculation: $\Gamma_1 = \Gamma_2 = 1$; $\Gamma' = 0$; $\gamma_1 = \gamma_2 = 2\pi$; $\gamma' = 0.4\pi$; $\Omega_1 = \Omega_2 = 4\pi$; $\Omega' = 0.2\pi$; $\Delta_1 = \Delta_2 = 0$; t = 2.5. Middle: Integrate over optical inhomogeneous width of 20, in steps of 0.4. Bottom: Integrate over spin inhomogeneous width of 20, in steps of 0.4. b) Calculated profile of 3L2F resonance. All parameters are the same as in a), except that $\Omega_2 = 0$.

Fig. 10: Calculated profile of 3L3F resonance for varying spin Rabi frequencies: from top to bottom, $\Omega' = 0.2\pi$, 0.4π, 0.8π. All other parameters are the same as in the middle trace of Fig. 9a).

Fig. 11: Calculated profile of 3L3F resonance for varying optical Rabi frequencies: from top to bottom, $\Omega_1 = \Omega_2 = 2\pi, 4\pi, 6\pi$. All other parameters are the same as in the middle trace of Fig. 9a).

Fig. 12: Calculated profile of 3L3F resonance for varying spin phase relaxation rates: from top to bottom, $\gamma' = 0.2\pi, 0.4\pi, 0.8\pi$. All other parameters are the same as in the middle trace of Fig. 9a).

Fig. 13: Calculated profile of 3L3F resonance for varying optical phase relaxation rates: from top to bottom, $\gamma_1 = \gamma_2 = 1\pi, 2\pi, 4\pi$. All other parameters are the same as in the middle trace of Fig. 9a).

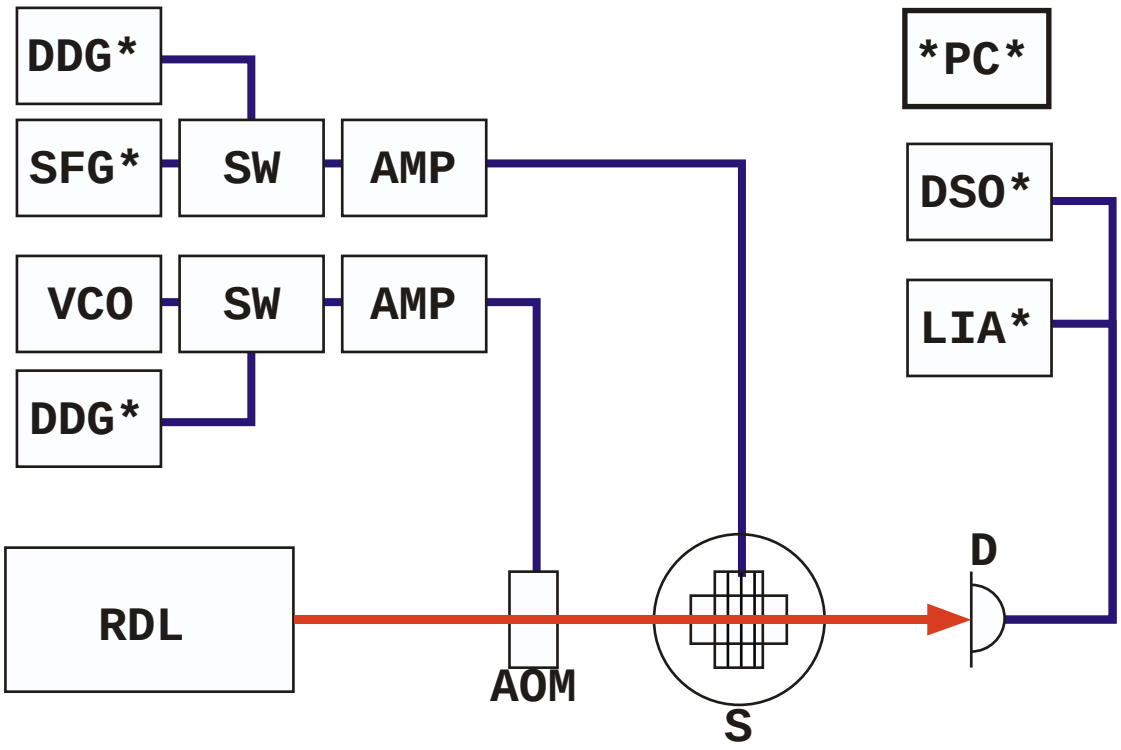

[M.K. Kim, et al. Fig. 1]

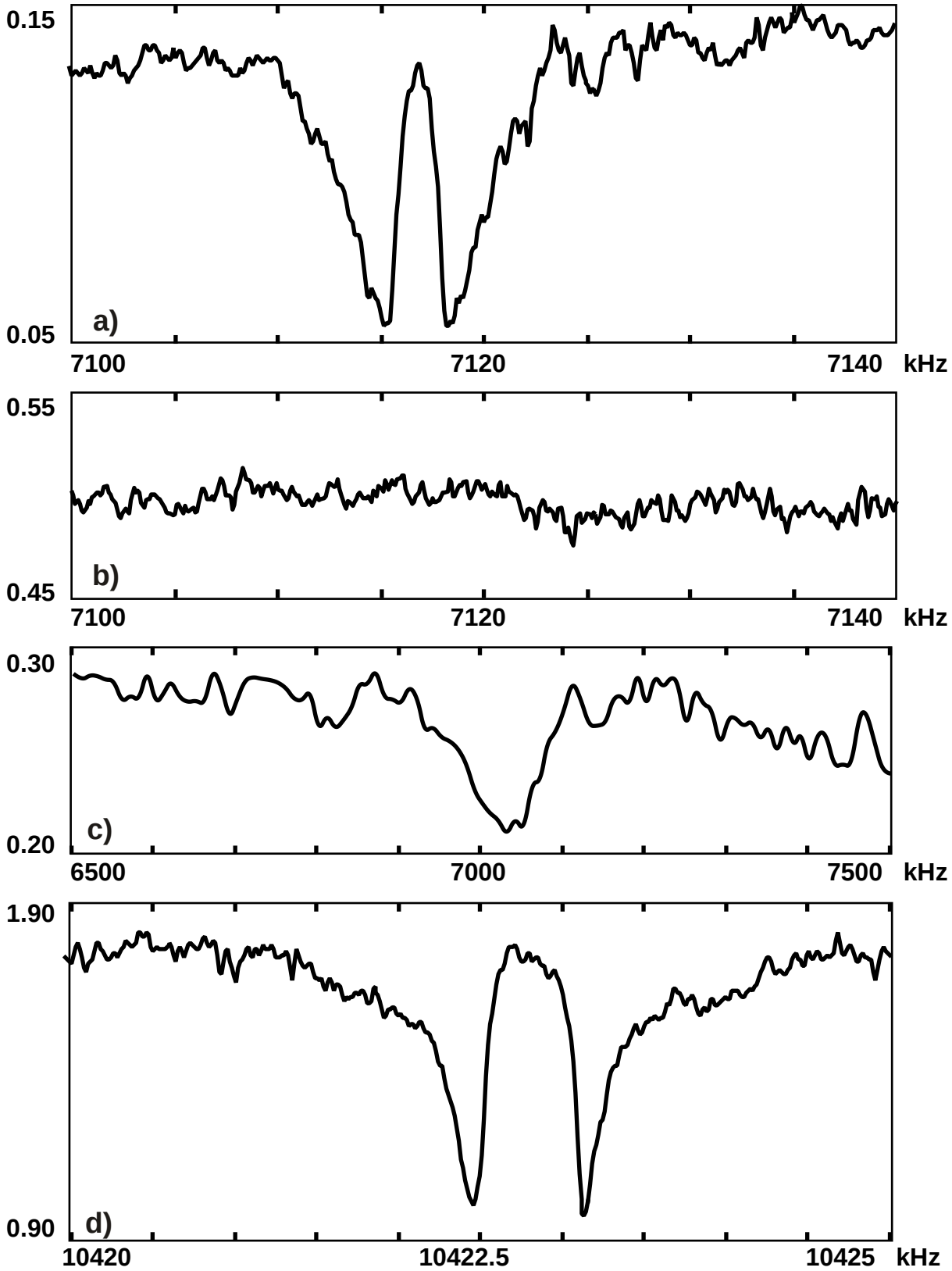

[M.K. Kim, et al. Fig. 2]

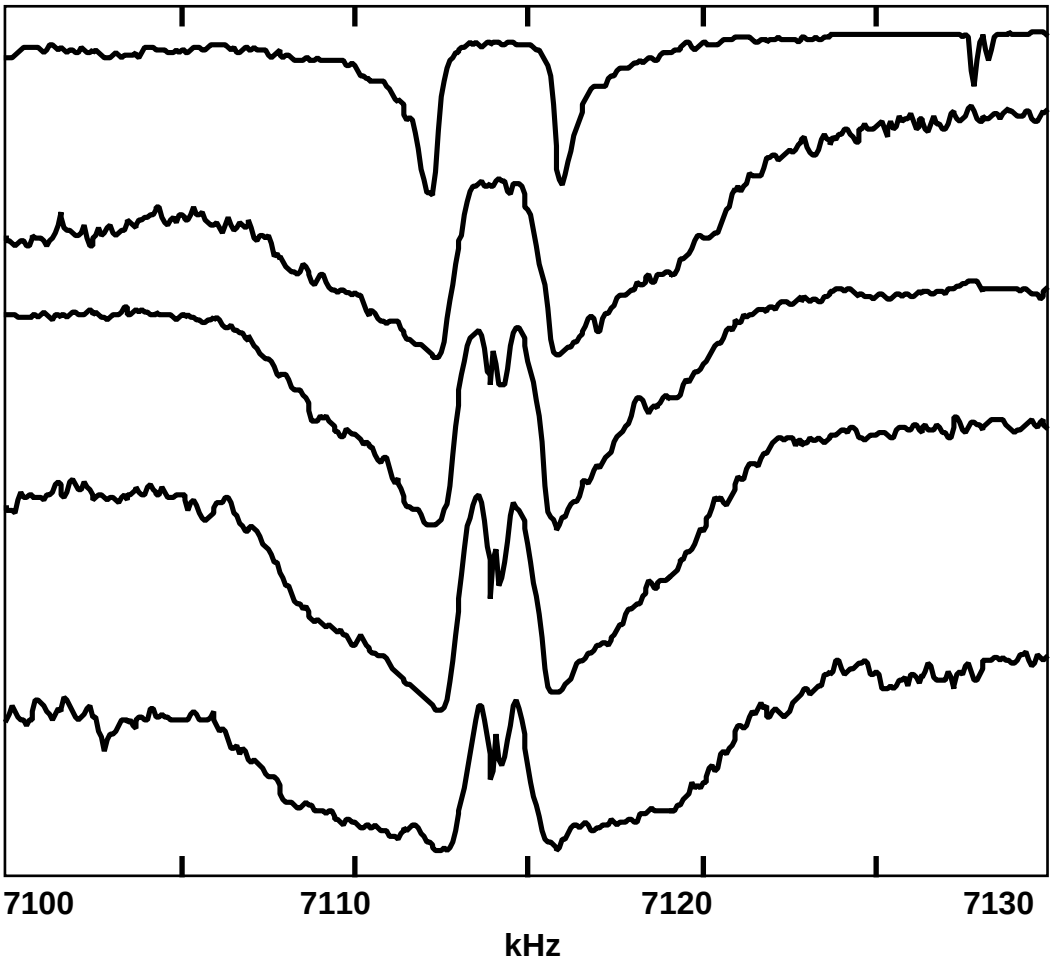

[M.K. Kim, et al. Fig. 3]

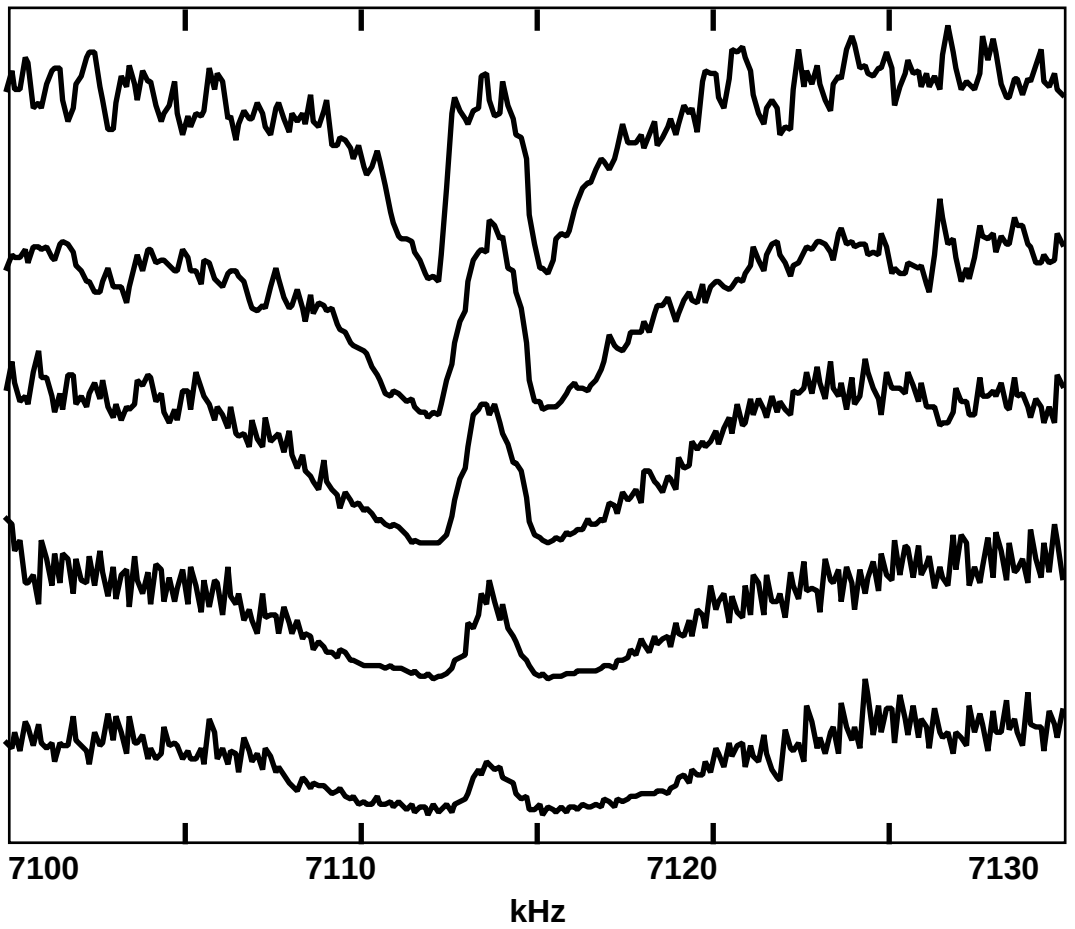

[M.K. Kim, et al. Fig. 4]

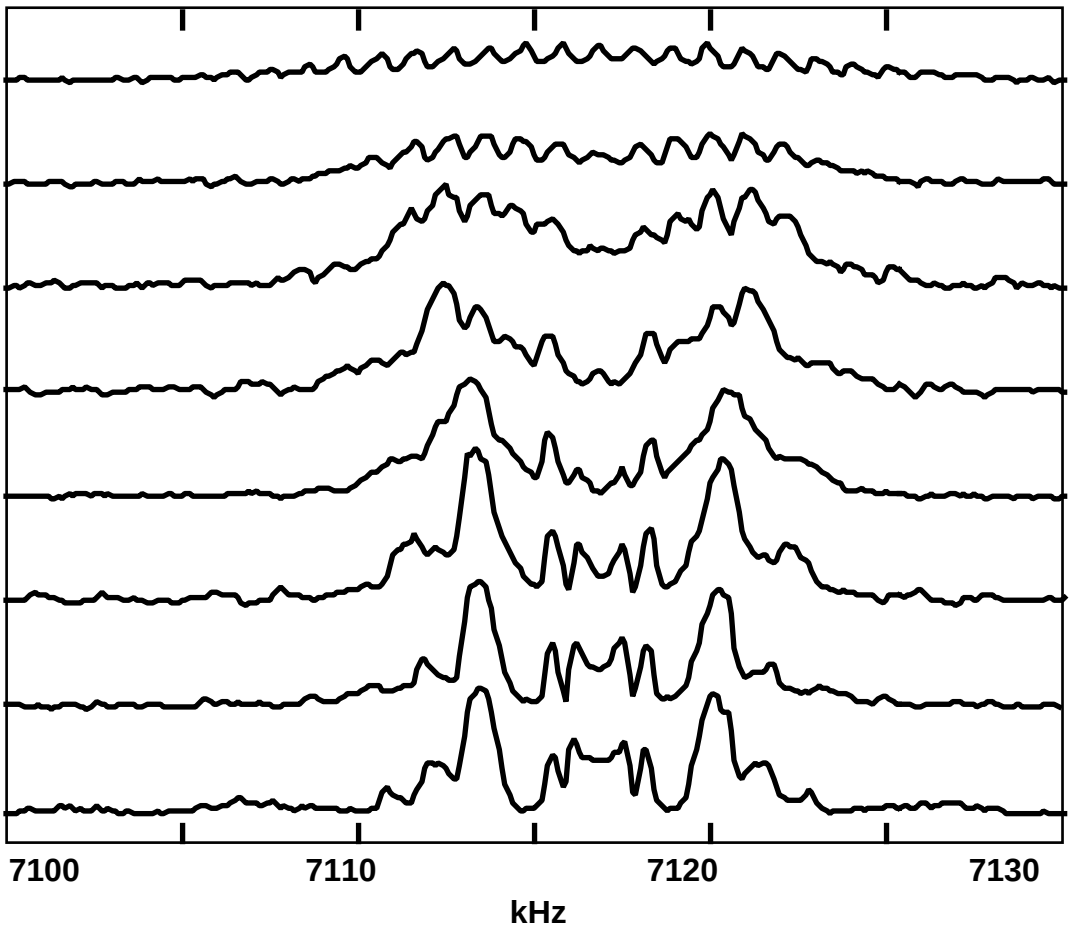

[M.K. Kim, et al. Fig. 5]

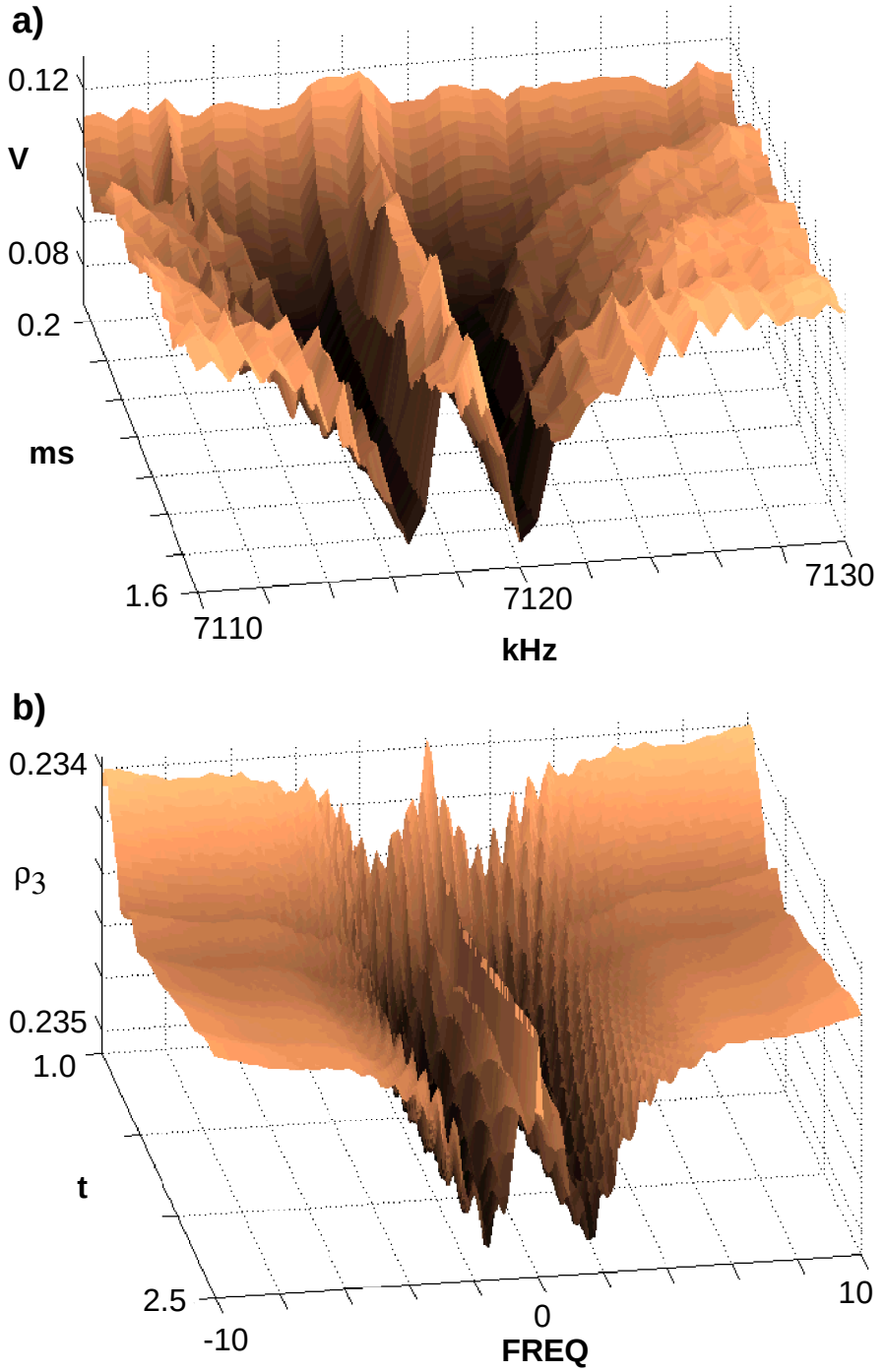

[M.K. Kim, et al. Fig. 6]

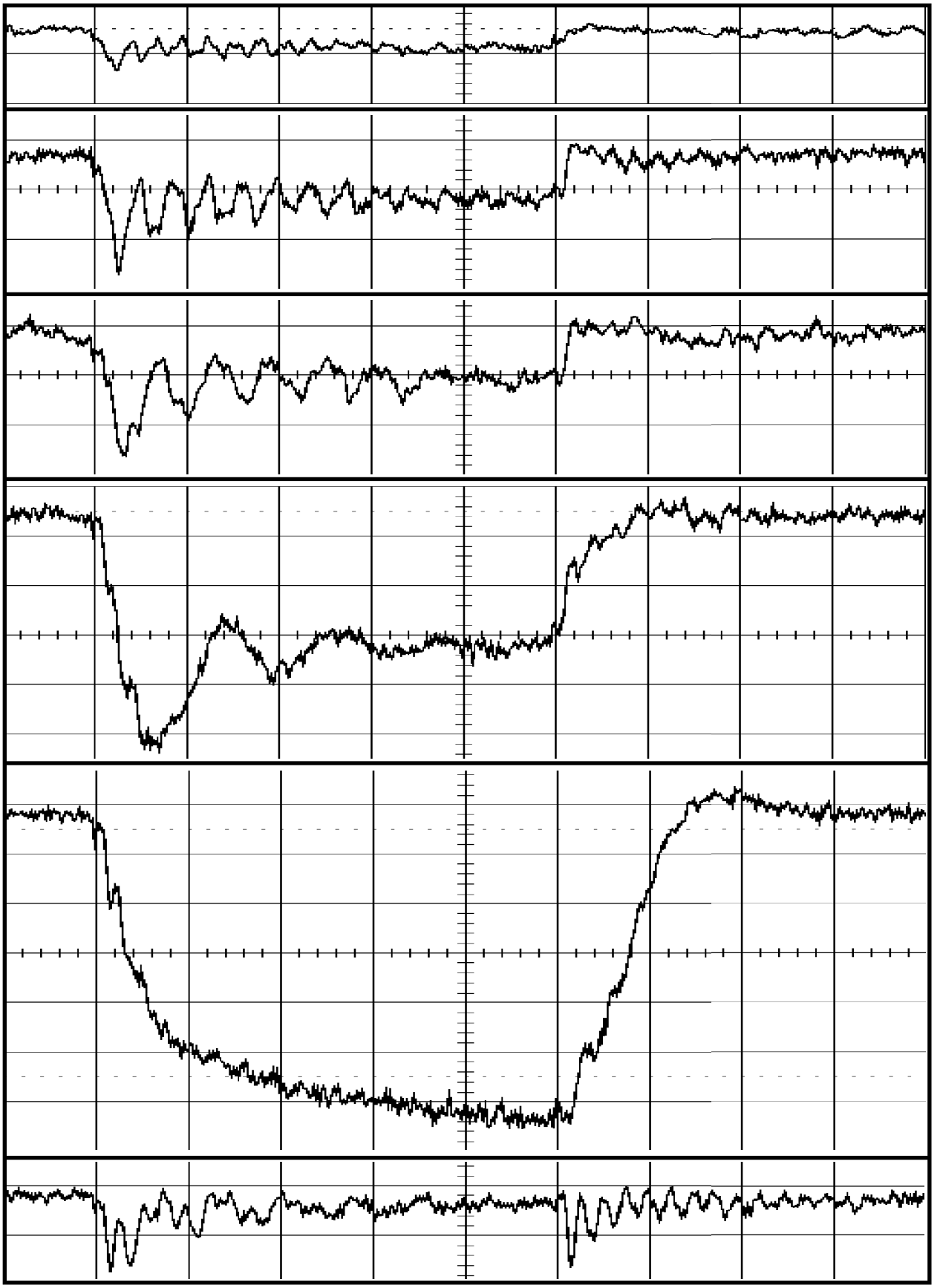

[M.K. Kim, et al. Fig. 7]

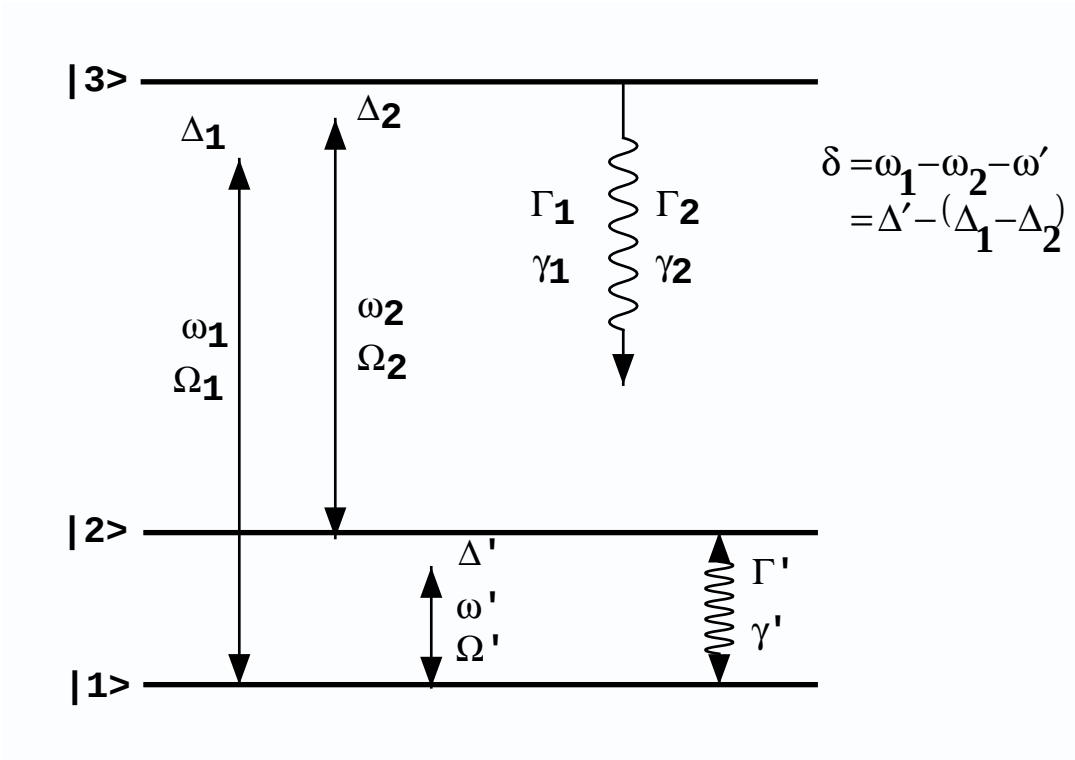

[M.K. Kim, et al. Fig. 8]

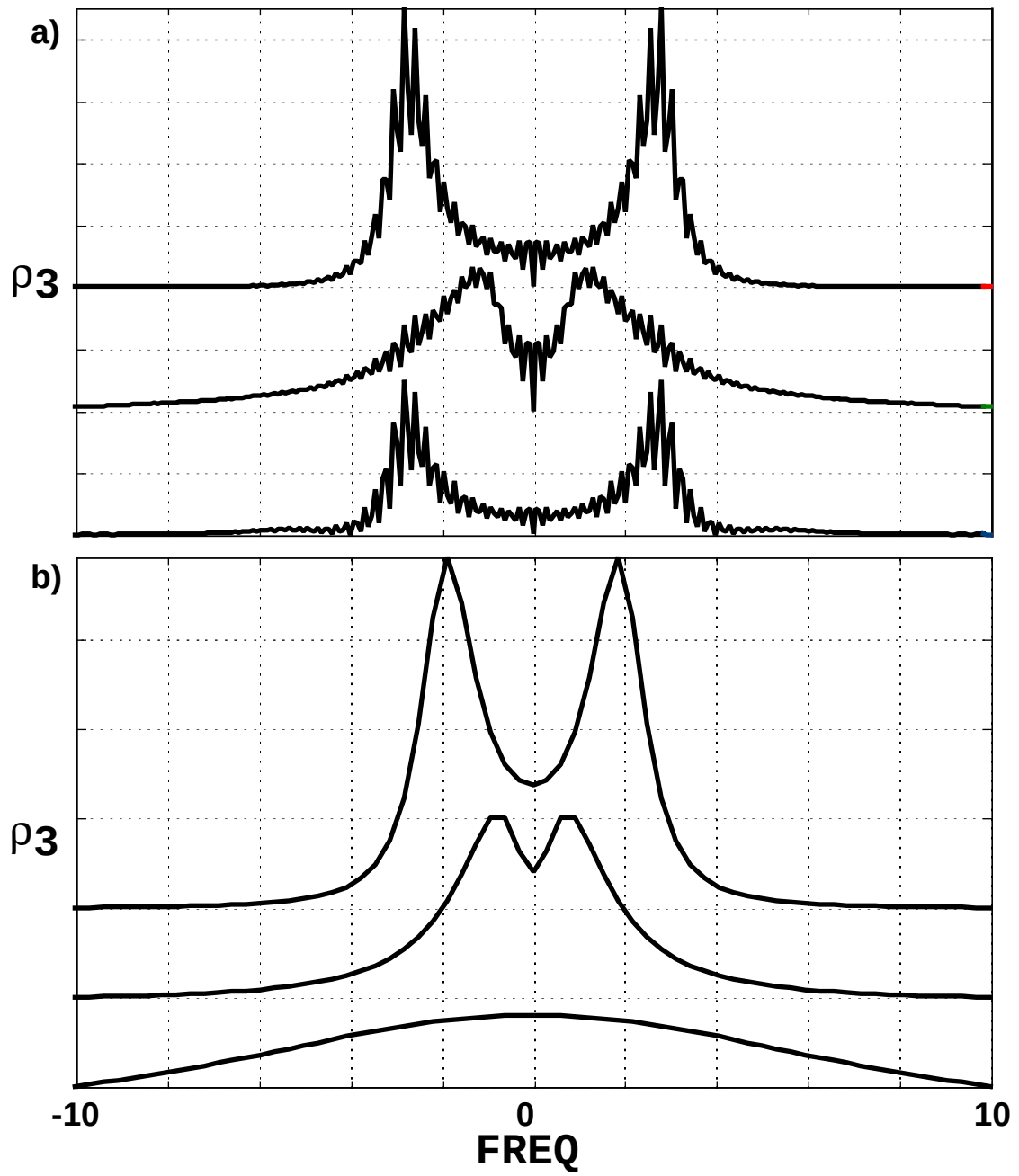

[M.K. Kim, et al. Fig. 9]

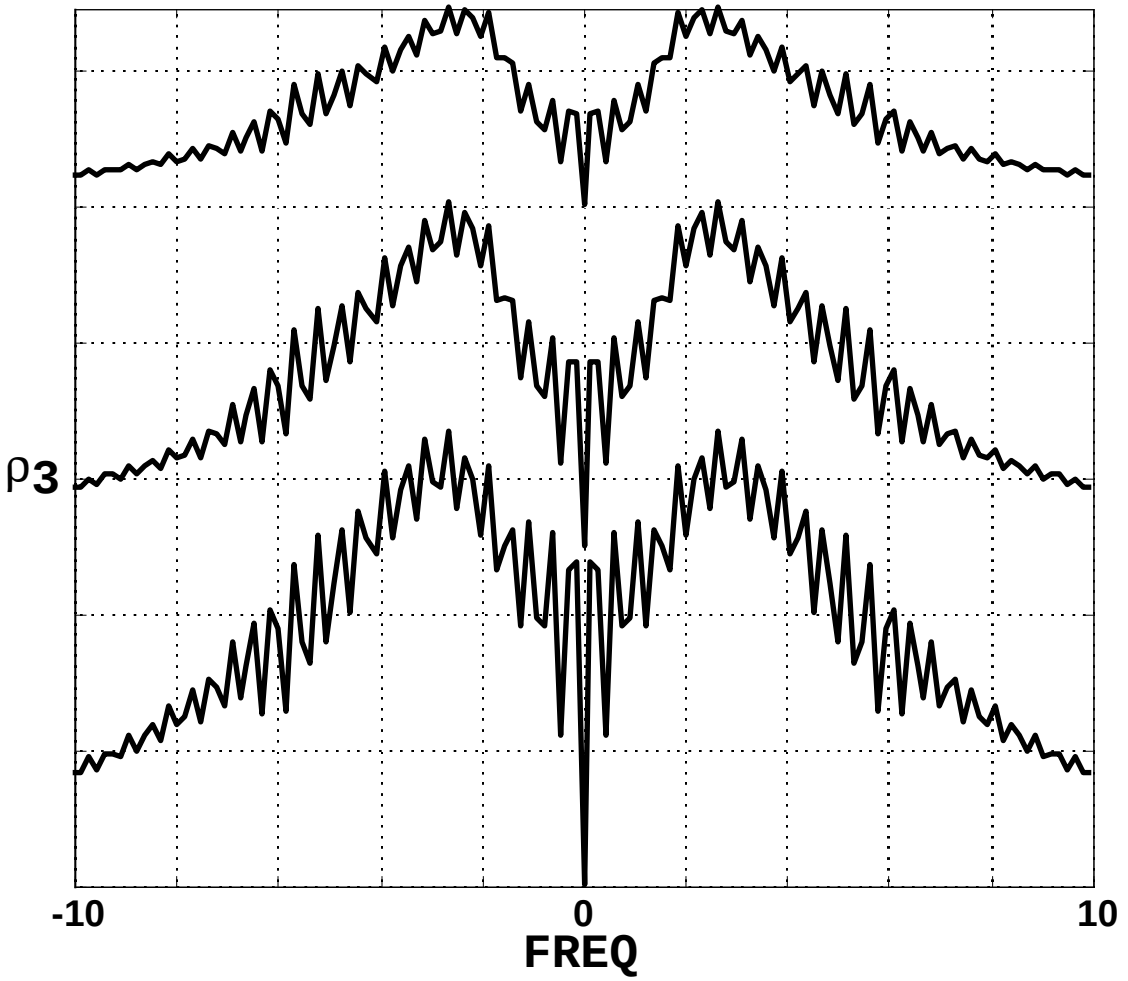

[M.K. Kim, et al. Fig. 10]

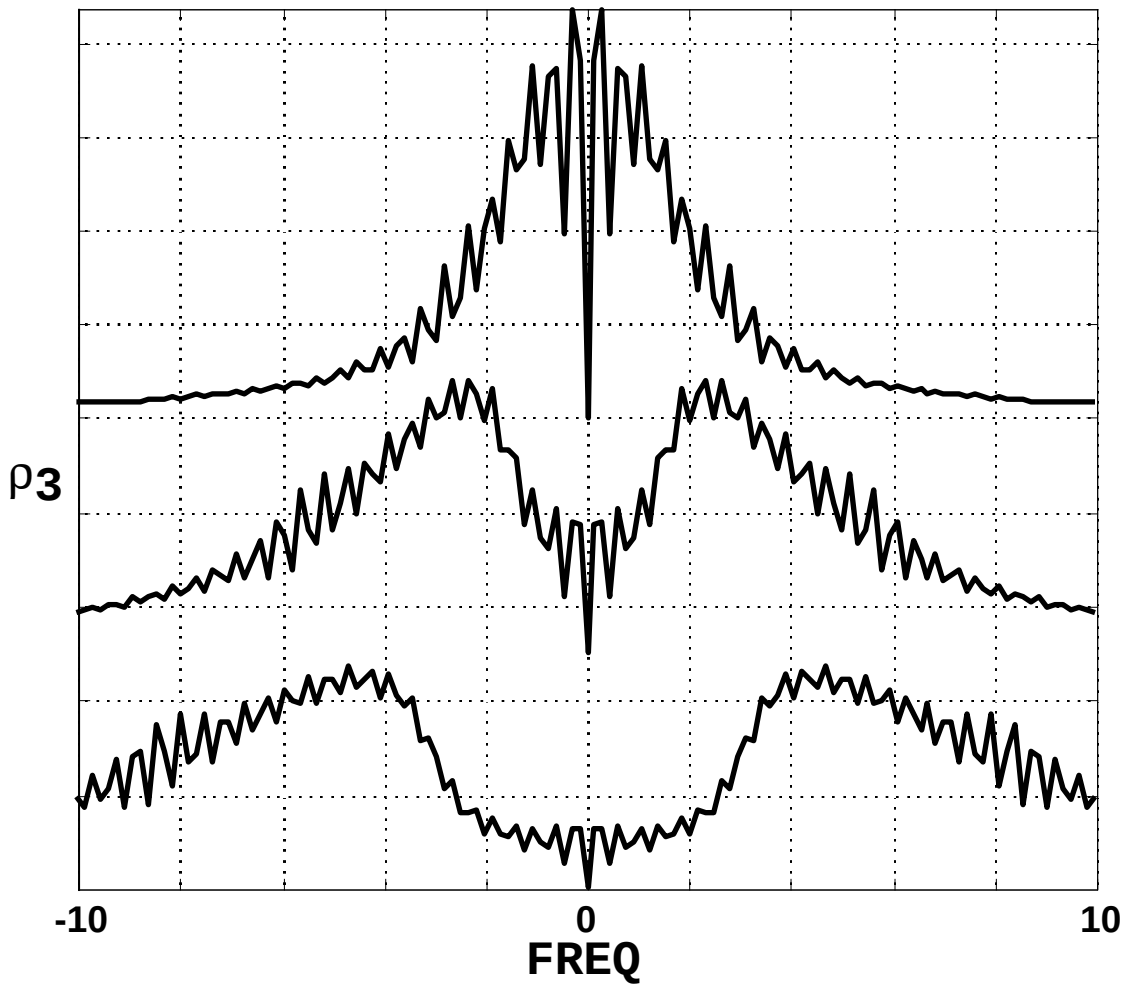

[M.K. Kim, et al. Fig. 11]

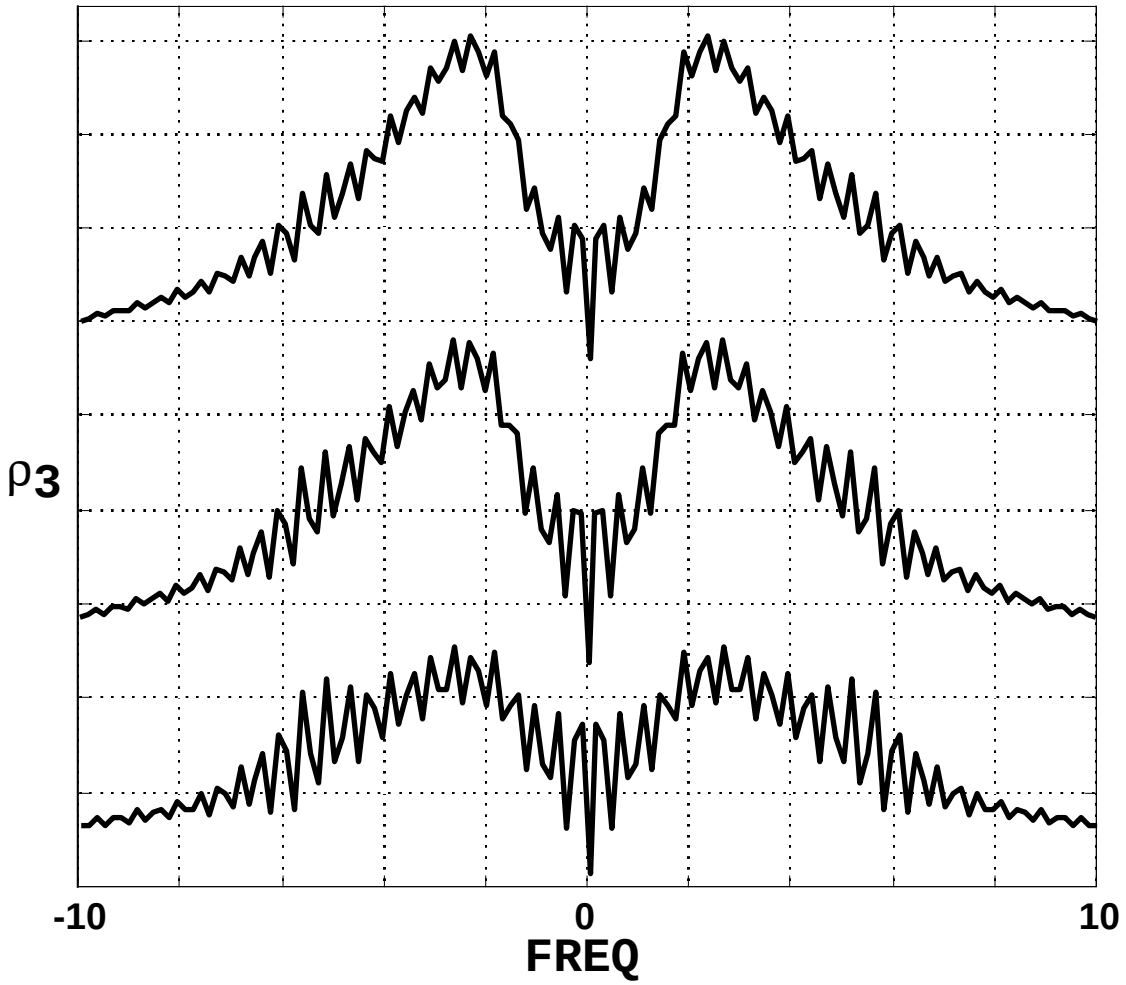

[M.K. Kim, et al. Fig. 12]

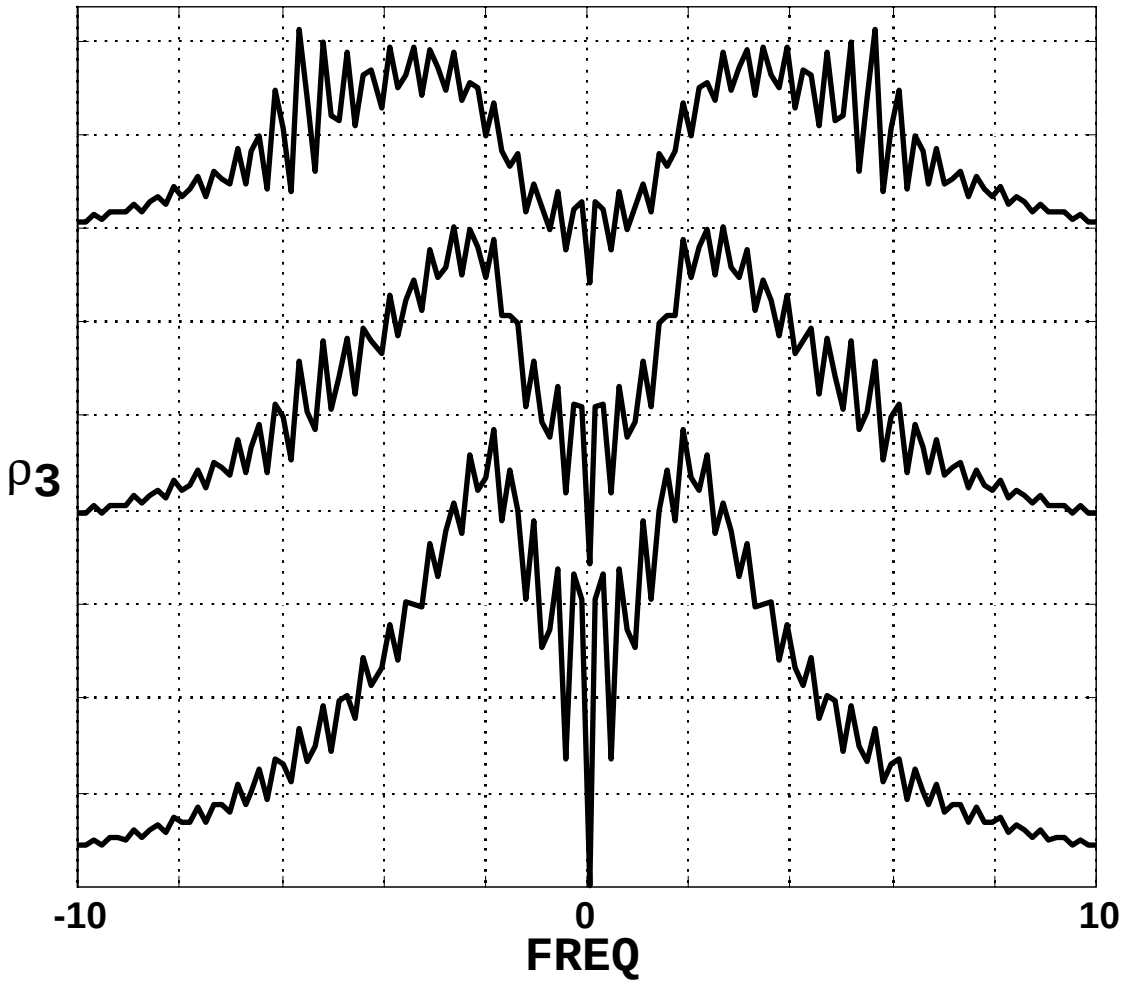

[M.K. Kim, et al. Fig. 13]